Cytoprotective metal-organic frameworks for anaerobic bacteria

Zhe Ji[a,b,c,1], Hao Zhang[a,1], Hao Liu[a], Omar M. Yaghi[a,b,c,d,2], and Peidong Yang[a,b,c,e,f,2]

[a]Department of Chemistry, University of California, Berkeley, CA 94720; [b]Materials Sciences Division, Lawrence Berkeley National Laboratory, Berkeley, CA 94720; [c]Kavli Energy NanoSciences Institute, Berkeley, CA 94720; [d]King Abdulaziz City of Science and Technology, 11442 Riyadh, Saudi Arabia; [e]Department of Materials Science and Engineering, University of California, Berkeley, CA 94720; and [f]Chemical Sciences Division, Lawrence Berkeley National Laboratory, Berkeley, CA 94720

Contributed by Peidong Yang, August 24, 2018 (sent for review June 4, 2018; reviewed by Jinwoo Cheon and William R. Dichtel)

We report a strategy to uniformly wrap *Morella thermoacetica* bacteria with a metal-organic framework (MOF) monolayer of nanometer thickness for cytoprotection in artificial photosynthesis. The catalytic activity of the MOF enclosure toward decomposition of reactive oxygen species (ROS) reduces the death of strictly anaerobic bacteria by fivefold in the presence of 21% O_2, and enables the cytoprotected bacteria to continuously produce acetate from CO_2 fixation under oxidative stress. The high definition of the MOF–bacteria interface involving direct bonding between phosphate units on the cell surface and zirconium clusters on MOF monolayer, provides for enhancement of life throughout reproduction. The dynamic nature of the MOF wrapping allows for cell elongation and separation, including spontaneous covering of the newly grown cell surface. The open-metal sites on the zirconium clusters lead to 600 times more efficient ROS decomposition compared with zirconia nanoparticles.

cell wrapping | metal-organic frameworks | anaerobic bacteria | artificial photosynthesis | reactive oxygen species

Anaerobic bacteria have long been bred and used for fermenting organic matter in the absence of O_2 to produce value-added chemicals (ethanol, acetic acid, lactic acid, acetone, and butanol) (1). Recent work on artificial photosynthesis takes advantage of the autotropic metabolism of these bacteria by employing CO_2 as the only carbon feed along with solar energy to produce fuels and chemicals (2–7). Although these studies show promise, the evolution of O_2 and reactive oxygen species (ROS) at the anode along with fuel generation are detrimental to the metabolism of anaerobic bacteria. Addressing this inherent vulnerability to oxidative stress will expand the range and conditions for implementing a truly productive artificial photosynthesis. In this article, we show that by wrapping a semiconductor-sensitized anaerobic bacteria (*Moorella thermoacetica*) with a monolayer of a metal-organic framework (MOF), CO_2 was converted to acetate twice as long as that observed without such wrapping. We find a fivefold decrease in death of the wrapped bacteria when subjected to an O_2 environment (21%), and that they are also capable of reproduction without loss of the MOF. It is well established that the O_2 species can be converted to H_2O_2 at the cell membrane (8). In our system, this O_2-H_2O_2 conversion is followed by H_2O_2 decomposition on the zirconium oxide units of the MOF. This sequence of reactions, being mediated by the MOF, prevents the generation and accumulation of ROS, known to be detrimental to the bacteria, and therefore dramatically elongates the lifetime in oxidative environment. The high definition of the MOF monolayer structure allowed us to confirm that the Zr^{4+} of the MOF is bonded to the phosphate units on the cell wall, and that the dynamic chemistry of this bonding is the key to the observed increase in lifetime of the bacteria, effectiveness of the wrapping, and the facility of their reproduction.

It is known that bacteria can be coated with polymers, inorganic nanoparticles, and MOFs to enhance their viability under radiation, thermal, and mechanical stress (9–15), but not to address the critical issue of the oxidative stress in artificial photosynthesis. These coatings suffer from a complicated synthetic procedure that yields either poor coverage or stiff shells hundreds of nanometers in thickness, which trap cells in dormant state. As such, the protection provided by these materials is only temporary because the material coating needs to be repeated every time a new batch of cells is introduced. The fact the bacteria we report here were wrapped with only 1–2-nm MOF layer and the bonds at the bacteria–MOF interface are dynamic, leads to facile reproduction and maintains protection against oxidative stress. It is worth noting that the excess MOF in the culture media can wrap over newly grown cell surfaces to pass on this protection over generations of anaerobes.

Results and Discussion

In this study, we chose the MOF $[Zr_6O_4(OH)_4(BTB)_2(OH)_6(H_2O)_6$; BTB = 1,3,5-benzenetribenzoate] (Fig. 1*A*) for cell wrapping because the constituting zirconium clusters are of low toxicity and high stability. The fact that these clusters can be connected by BTB linkers into self-supporting monolayer (16) further makes this material an ideal candidate. To build the bacteria–MOF construct, we developed a strategy through adding a presynthesized MOF monolayer into the culture media of bacteria (Fig. 1*B*).

Significance

Culturing bacteria to produce desired chemicals has long been practiced in human history, and has recently being taken as a promising approach to sustainable energy when this process is driven by sunlight and fed by CO_2 as the only carbon source. Among these chemical-producing microbes are anaerobic bacteria, inherently susceptible to O_2 and reactive oxygen species that are inevitably generated on anodes. Here, we provide cytoprotection against such oxidative stress by wrapping bacteria with an artificial material, metal-organic frameworks (MOFs), which significantly enhances the lifetime of anaerobes in the presence of O_2, and maintains the continuous production of acetic acid from CO_2. The ultrathin nature of the MOF layer allows for cell reproduction without loss of this cytoprotective material.

Author contributions: Z.J., H.Z., O.M.Y., and P.Y. designed research; Z.J., H.Z., and H.L. performed research; Z.J., H.Z., and H.L. contributed new reagents/analytic tools; Z.J., H.Z., O.M.Y., and P.Y. analyzed data; and Z.J., H.Z., O.M.Y., and P.Y. wrote the paper.

Reviewers: J.C., Yonsei University; and W.R.D., Northwestern University.

Conflict of interest statement: O.M.Y and William R. Dichtel were part of the same MURI team until 2017; they did not work together or co-publish.

Data deposition: The atomic coordinates and structure factors have been deposited in the Cambridge Structural Database, https://www.ccdc.cam.ac.uk/ (accession no. CCDC 1863035).

[1]Z.J. and H.Z. contributed equally to this work.

[2]To whom correspondence may be addressed. Email: yaghi@berkeley.edu or p_yang@berkeley.edu.

This article contains supporting information online at www.pnas.org/lookup/suppl/doi:10.1073/pnas.1808829115/-/DCSupplemental.

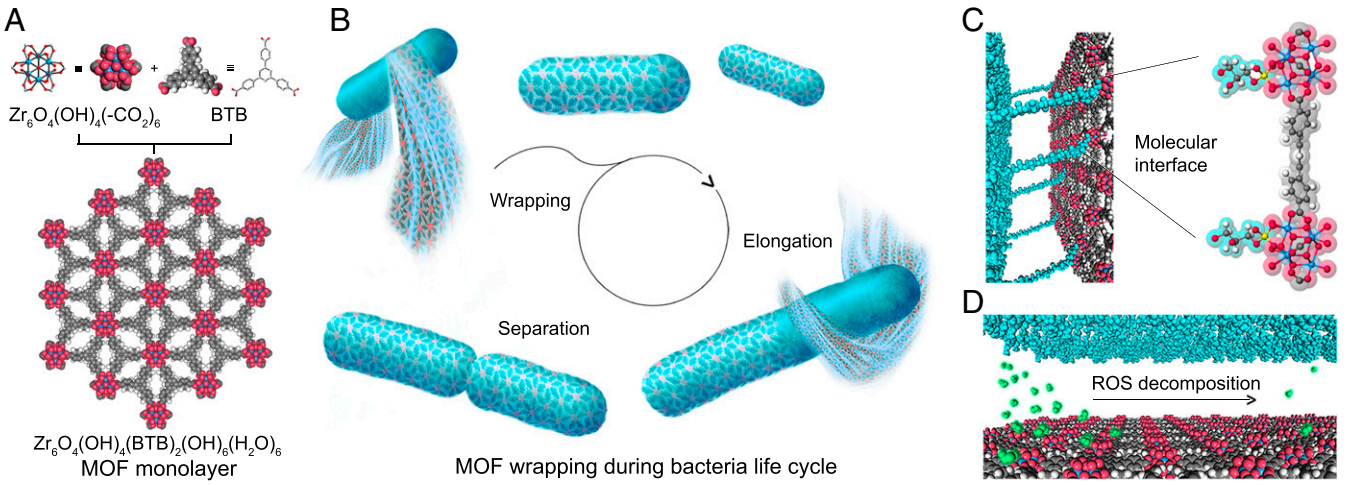

Fig. 1. Design and synthesis of the *M. thermoacetica*–MOF wrapping system. (*A*) The MOF monolayer comprises 6-connected $Zr_6O_4(OH)_4(\text{-}CO_2)_6$ cluster and trigonal BTB linker. (*B*) The monolayer of MOF spontaneously wraps around *M. thermoacetica*, allowing for elongation and separation of cells, during which newly formed cell surface is wrapped in situ by an excess of MOF in the culture medium. (*C*) The molecular structure at the interface illustrates the multivalent coordination bonds form between the inorganic clusters of MOF and the phosphate moieties of teichoic acid on cell wall. (*D*) Decomposition of ROS by the MOF monolayer coating on cell surface. In the space-filling model, atoms of cell wall and ROS are represented in cyan and green spheres, respectively. Hydrogen atoms on zirconium clusters are omitted for clarity. Color code: blue, Zr; red, O; gray, C; white, H; yellow, P.

This postsynthetic method, in contrast to the in situ growth of MOF shells on bacteria (10), allows the spontaneous wrapping to occur around the newly grown cell surface, facilitated by the coordination bond between the zirconium cluster and teichoic acid on cell wall (Fig. 1*C*). The accomplished MOF wrapping is envisioned to serve as a cytoprotective layer due to its catalytic activity toward ROS decomposition reaction (Fig. 1*D*).

The MOF monolayer was obtained using an established method (16). Transmission electron microscopy (TEM) confirms the formation of the self-supporting MOF monolayer with lateral dimensions of micrometers (Fig. 2*A*). Early stationary stage *M. thermoacetica*, cultured in heterotrophic medium, was centrifuged down and redispersed together with MOF monolayers in the autotrophic culture medium. Upon gentle shaking, spontaneous wrapping was afforded over the course of 1 h. The morphology of the resulting wrapping systems, *M. thermoacetica*–MOF, was examined by TEM (Fig. 2*B* and *SI Appendix*, Fig. S1 *A–E*), scanning transmission electron microscopy (STEM) (Fig. 2*C* and *SI Appendix*, Fig. S1*F*), and scanning electron microscopy (SEM) (Fig. 2*D* and *SI Appendix*, Fig. S2), confirming that the bacteria were wrapped with ultrathin layers covering and further protruding from the whole body of the cell. The chemical composition of the wrapping construct was analyzed using energy-dispersive X-ray spectroscopy (EDXS) mapping (Fig. 2 *E–H*). The overlapping region of atomic distribution between zirconium, carbon, sulfur, and phosphorus indicates the presence of MOF over the cell body. Structured illumination microscopy was employed to assess the structure of the heterogeneous wrapping system. For this experiment, we labeled MOF monolayer and bacteria with fluorescein (*SI Appendix*, Fig. S3) and intracellular gold nanocrystals, emitting green and red fluorescence, respectively. The rebuilt 3D images (*SI Appendix*, Fig. S4) display a core–shell structure, further corroborating that the bacteria were wrapped by MOF.

The crystallinity of MOF and *M. thermoacetica*–MOF were examined by powder X-ray diffraction (PXRD). The obtained PXRD patterns of the MOF soaked in culture media and the final wrapping construct *M. thermoacetica*–MOF were found to be in good agreement with that of the as-synthesized framework (Fig. 2*I*), confirming that the MOF remained intact during the cell wrapping process. The presence of the MOF was further confirmed by Fourier transform infrared (FTIR) spectra, where *M. thermoacetica*–MOF features aromatic C = C (1,407 cm^{-1}) and C-H stretches (856 and 777 cm^{-1}) of the BTB linker (*SI Appendix*, Fig. S5). The weight percent of MOF monolayer in the resulting wrapping construct was determined by inductively coupled plasma atomic emission spectroscopy (ICP-AES) and found to be 6.0 ± 0.9%.

The spontaneous wrapping of MOF monolayer over bacteria is facilitated by the coordination sites on zirconium clusters where hydroxyl and water ligands can be readily replaced by phosphate groups (17) of teichoic acid on the cell surface (18, 19). To have the cell surface as the only phosphate-containing ligand, β-glycerophosphate, a nutrient component, was excluded from the culture medium during the wrapping process for structural assessment. FTIR spectra of the resulting wrapping system (*M. thermoacetica*–MOF-NP) exhibits the appearance of a peak at 839 cm^{-1}, which does not belong to either bacteria or MOF alone (Fig. 2*J*). To identify its chemical nature, a molecular analog of the proposed *M. thermoacetica*–MOF fragment, zirconium dimethylphosphate (ZrDMPO), was synthesized and used as a model compound. The structure of ZrDMPO was solved by single-crystal X-ray diffraction (SXRD) (*SI Appendix*, Fig. S6 and Tables S1 and S2) and comprised two oxygen atoms of DMPO coordinating to adjacent zirconium ions in a bidentate fashion. This very bonding was found to exhibit a (Zr)-O-P stretch at 839 cm^{-1} in the FTIR spectrum (20), consistent with the peak that emerged from that of *M. thermoacetica*–MOF-NP (Fig. 2*J*). The coordination of β-glycerophosphate to the zirconium cluster occurs when MOF is soaked alone in the culture media and displays a (Zr)-O-P stretch (832 cm^{-1}), which contributes to the broad peak at the same position in the FTIR spectra of *M. thermoacetica*–MOF. This result indicates the presence of both β-glycerophosphate and cell surface bonding to the zirconium clusters when the wrapping is processed in the complete culture media, between which the competition can enable a dynamic wrapping that allows for the elongation and separation of the cell wall. The presence of coordination bonds between phosphate moieties on the cell surface and zirconium clusters was corroborated by X-ray photoelectron spectroscopy (XPS) (Fig. 2*K* and *SI Appendix*, Fig. S7). The P 2p spectrum of *M. thermoacetica*–MOF-NP exhibits a binding energy shift from 132.8 to 133.1 eV relative to the bare bacteria, analogous to that of the model compound ZrDMPO with P 2p binding energy of 133.2 eV.

To assay the biocompatibility of the MOF monolayer, heterotrophic growth of *M. thermoacetica* cultured under anaerobic conditions was profiled by counting colony-formed units (cfu). *M. thermoacetica*–MOF was observed to exhibit a growth curve consistent with that of the bare bacteria (Fig. 3*A*), which reveals

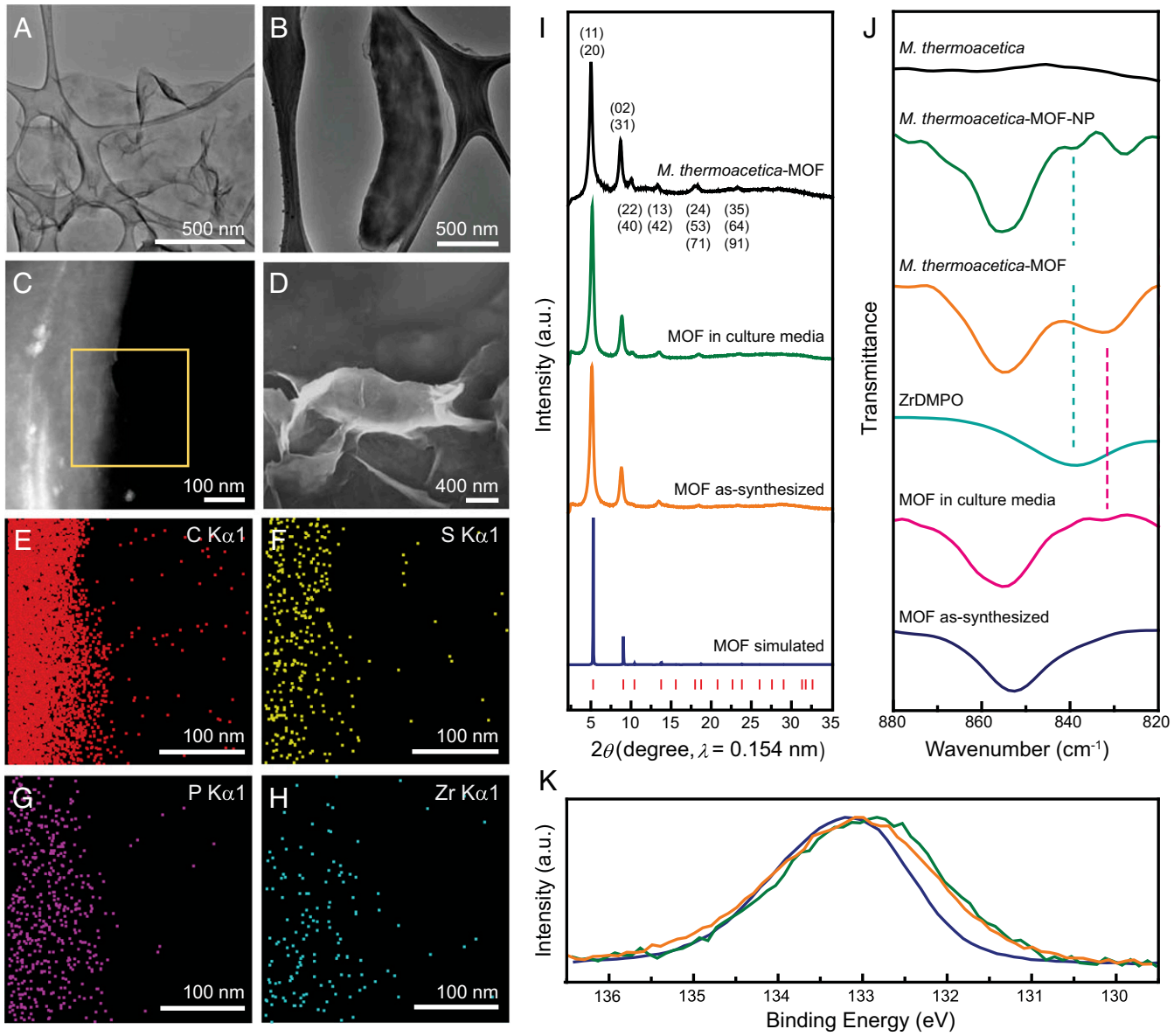

Fig. 2. Structural characterization of *M. thermoacetica*–MOF. (*A*) TEM image of MOF monolayer. TEM image (*B*), High-angle annular dark-field STEM image (*C*), and SEM image (*D*) of *M. thermoacetica*–MOF. EDS mapping of the selected region labeled by yellow square in *C* confirms the presence of carbon (*E*), sulfur (*F*), phosphorus (*G*), and zirconium (*H*) on the edge of *M. thermoacetica*–MOF. (*I*) PXRD pattern and Bragg position (red lines) of *M. thermoacetica*–MOF, MOF soaked in culture media, MOF as-synthesized, and the modeled structure. (*J*) FTIR spectra of *M. thermoacetica*, *M. thermoacetica*–MOF, *M. thermoacetica*–MOF cultured in phosphate-free medium (-NP), the model compound ZrDMPO, MOF soaked in culture media, and MOF as-synthesized. Peaks at 839 and 832 cm^{-1} are labeled with dashed lines in cyan and magenta, respectively. (*K*) P 2p spectra obtained by XPS of ZrDMPO (blue), *M. thermoacetica*–MOF-NP (orange), and *M. thermoacetica* (green).

that the MOF wrapping maintains cell life and their reproductive capacity. This finding was supported by the observation that MOF monolayer permits the transportation of small molecules necessary for cell growth (*SI Appendix*, Fig. S8). The reproduction process of *Escherichia. coli* wrapped by MOF monolayer in the microfluidic cell was recorded in a time-lapse movie by labeling MOF with green fluorescence (Fig. 3*B* and Movies S1 and S2). The motion of the MOF enclosure was tracked and found to move in accordance with the elongation and separation of the cell surface, and carried by bacteria of next generations. When excess MOF monolayers are present in the culture media, the newly grown cell surface could be spontaneously covered. Therefore, the in situ wrapping process allows cell reproduction and guarantees the retention of cytoprotection in future generations.

Classified as strict anaerobes, several acetogenic bacteria used in artificial photosynthesis, including *M. thermoacetica* (6), have been reported to only tolerate low levels of O_2 (8, 21, 22). To investigate the cytoprotective effect of MOF enclosure on anaerobes under oxidative stress, *M. thermoacetica* cultures were subject to O_2 after reaching a stationary phase. It was observed that *M. thermoacetica* equipped with MOF enclosure cultured in 21% O_2 environment exhibit a high viability of 76 ± 8% after 2 d, which is comparable to the survival ratio of 83 ± 7% cultured under anaerobic conditions (Fig. 3*C*). In contrast, the population of the bare bacteria without this artificial enhancement decayed to 50 ± 7% when exposed to the same level of O_2, corresponding to a fivefold increase in death. Additionally, the defense of MOF enclosure against H_2O_2, a predominant ROS, was analyzed by feeding H_2O_2 into the culture media at the concentrations of 1,

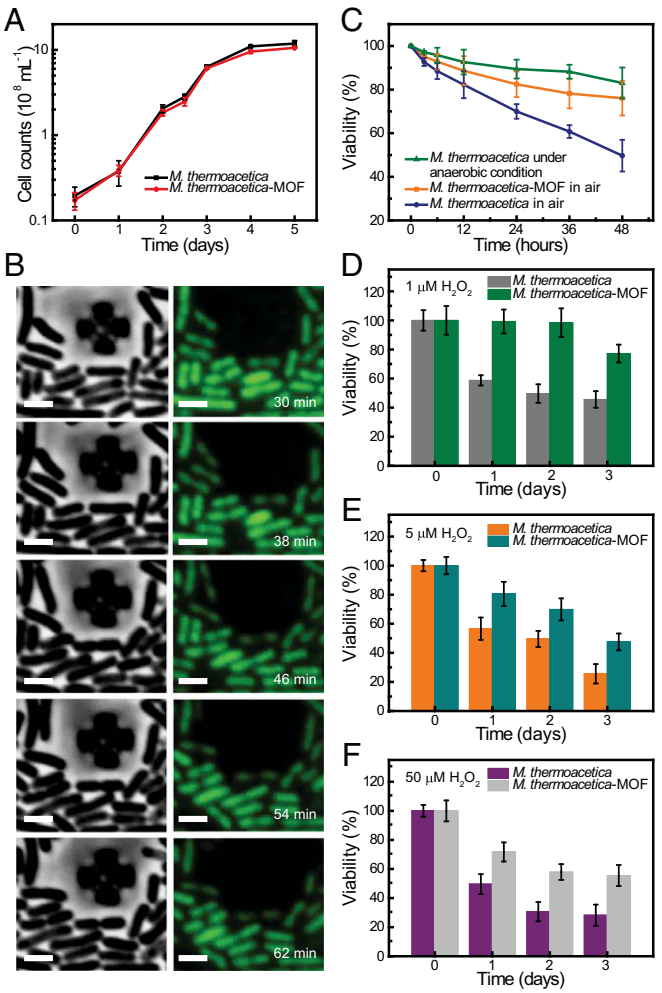

Fig. 3. MOF monolayer enclosure allows for the reproduction of bacteria and enhances their viability under oxidative stress. (*A*) Heterotrophic growth curves of *M. thermoacetica* and *M. thermoacetica*–MOF under the anaerobic condition. (*B*) Snapshots of the division process of *E. coli*–MOF captured in dark field (*Left*) and fluorescence field (*Right*). (Scale bars: 1 μm.) (*C*) Cell population decay curves of *M. thermoacetica* and *M. thermoacetica*–MOF in air, and bare *M. thermoacetica* under anaerobic conditions. The viability of *M. thermoacetica* and *M. thermoacetica*–MOF in media containing H_2O_2 at concentrations of 1 μM (*D*), 5 μM (*E*), and 50 μM (*F*). Error bars represent SD.

5, and 50 μM. The cytoprotective MOF was found to result in a significantly improved viability of *M. thermoacetica* in these H_2O_2 media (Fig. 3 *D*–*F*).

The protection against oxidative stress by the MOF monolayer might originate from its catalytic activity toward ROS decomposition due to the structural resemblance between zirconium clusters and active sites of zirconia (23). Mechanistic studies of this process were performed by measuring the H_2O_2 concentration in MOF media, determined according to the Ghormley triiodide method (24, 25), at different time intervals. An initial rapid decrease in H_2O_2 concentration was observed, which is ascribed to the physical adsorption of H_2O_2 on the MOF surface (Fig. 4*A*). Once the physical adsorption reaches its equilibrium, the catalytic decomposition of H_2O_2 becomes dominant, which shows a first-order rate dependence on H_2O_2, analogous to what is observed for zirconia (26). The catalytic activity of the MOF monolayer is further quantified by the second-order rate constant as $k_2 = 3.26 \pm 0.04 \times 10^{-9}$·m·s^{-1} (Fig. 4*B*), a number that is 28 times higher than zirconia nanoparticles when normalized by the number of zirconium atoms on the surface, and 600 times higher when normalized by mass (*Materials and Methods*). To further demonstrate the advantage of wrapping bacteria with the MOF monolayer, we compare the cytoprotection effects against oxidative stress by the MOF monolayer and zirconia nanoparticles. When adding the same amount of zirconia nanoparticles (mass based on Zr) into the culture media, the viability of *M. thermoacetica* remained the same and no cytoprotection effect was observed (*SI Appendix*, Fig. S10). Such comparison further highlights the efficient catalytic performance of the MOF monolayer and indicates the benefit of the proximity to the catalytic active sites in the wrapping system.

The catalytic performance of the MOF monolayer is vital to the enhanced tolerance of the anaerobes against oxidative stress. When anaerobes such as *M. thermoacetica* are exposed to O_2, H_2O_2 can be generated by NADH oxidase (8) on the cell membrane and diffuse into the cell. Once the amount of H_2O_2 exceeds the buffering capacity of glutathione, it poses a threat to cell survival by its transformation into toxic hydroxyl radical through Fenton's reaction. In our system, we demonstrate that the O_2-H_2O_2 conversion is followed by H_2O_2 decomposition on the zirconium oxide units of the MOF. This sequence of reactions, being mediated by the MOF, prevents the accumulation of ROS and therefore dramatically elongates the lifetime in oxidative environment. The enhanced tolerance of *M. thermoacetica* against oxidative stress holds the promise in facilitating the whole reaction of the photosynthesis of acetate from CO_2 in conjugation with oxygen evolution reaction. To show the proof of concept, into our previous photosynthetic biohybrid system (PBS) (6) was injected 2% O_2 to mimic the atmosphere of the whole photosynthetic reaction. It was found that the bare PBS without the cytoprotective MOF wrapping can only be functional to fix CO_2 into acetate within the first day (*SI Appendix*, Fig. S11). The short lifetime of PBS is due to the cytotoxicity of O_2 and ROS generated along with photosynthesis. In contrast, the MOF wrapping maintains the photosynthesis by PBS for 2.5 d under the same condition, and increases the productivity of acetate to 200%.

Materials and Methods

All starting material and solvents, unless otherwise specified, were obtained from Aldrich Chemical Co. and used without further purification.

Synthesis of MOF Monolayer $Zr_6O_4(OH)_4(BTB)_2(OH)_6(H_2O)_6$. The synthetic protocol was modified based on the reported literature (16). The obtained MOF dispersion was repeatedly washed by centrifugation with *N,N*-dimethylformamide (DMF) and then water. The washed MOF monolayer, as a white gel sitting at the bottom of the centrifuge tubes, was redispersed in 0.1 M HCl and heated at 90 °C overnight to remove formate ligands. The resulting suspension was filtrated over polyethersulfone membrane filters (pore size of 0.2 μm, STERLITECH) and washed with water. The filter cake, before getting dried, was redispersed in water and stored for further usage. The concentration of the obtained MOF monolayer dispersion in water was determined by measuring UV-vis spectroscopy. The absorption coefficient at 280 nm was found to be 0.10 mg^{-1}·L·cm^{-1} by quantifying zirconium amount

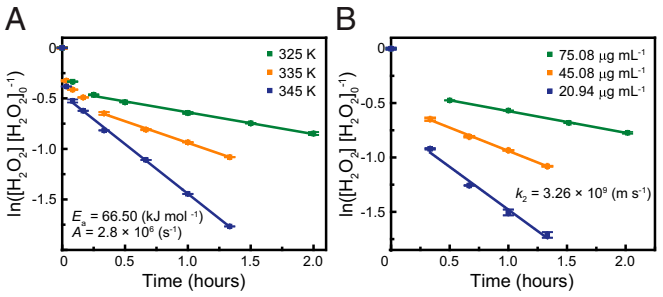

Fig. 4. The mechanism of protection against oxidative stress by MOF enclosure. Normalized concentration of H_2O_2 as a function of time in the decomposition reaction at different temperatures ([MOF] = 45.08 μg mL^{-1}) (*A*), and at different concentrations of MOF (335 K) (*B*). The Arrhenius activation energy E_a, frequency factor A, and the second-order rate constant k_2 were determined (*Materials and Methods* and *SI Appendix*, Fig. S9). Error bars represent SD.

using ICP-AES. This value was then referred for further usage in the quantification of this material.

Preparation of Heterotrophic Medium. The medium was prepared under anaerobic conditions with deionized water. The Hungate technique or an anaerobic chamber (Coy Laboratory Products, Inc.) was employed in all operations to prevent the exposure of anaerobic bacteria to oxygen. The recipe for a general broth is the same as before (6). To make the heterotrophic medium, 25 mL of 1 M glucose solution, 20 mL of 5 wt % Cys·HCl solution, 800 mg of β-glycerophosphate·2Na·xH_2O, 500 mg of yeast extract (BD Biosciences), and 500 mg of tryptone (BD Biosciences) were added into 1 L of the general broth and stirred until fully dissolved. Anaerobic media were then dispensed under a mixed atmosphere (80:20 mixture of N_2: CO_2) into 16 × 125-mm Balch-type anaerobic culture tubes (Chemglass Life Sciences) with butyl rubber stoppers and screw caps, and 18 × 150-mm Balch-type anaerobic culture tubes (Chemglass Life Sciences) with butyl rubber stoppers and aluminum crimp seals. Media were then autoclaved for 15 min at 121 °C before use.

Culturing *M. thermoacetica*. The initial inoculum of *M. thermoacetica* (American Type Culture Collection, ATCC 39073) was cultured in the heterotrophic medium, and the late log cultures were cryopreserved in a −80 °C freezer with 10% dimethyl sulfoxide as a cryoprotectant. To prepare *M. thermoacetica* cultures, 0.5 mL of the thawed cryopreserved stock of *M. thermoacetica* was inoculated in 10 mL of the anaerobic heterotrophic medium, and incubated with occasional agitation at 52 °C. The headspace of each tube was pressurized to 150 kPa with a flux of the mixed atmosphere (80:20 mixture of N_2:CO_2). After 2 d of growth (OD_{600} = 0.16), the culture was reinoculated at 5 vol % into fresh heterotrophic medium, and incubated at 52 °C. After the other 2 d of growth (OD_{600} = 0.38), the bacteria were centrifuged down at 860 × *g* for 10 min, washed, and resuspended in an equivalent volume of heterotrophic medium.

Wrapping MOF Monolayer Around *M. thermoacetica*. The bacteria culture in the heterotrophic medium was supplemented with MOF monolayer dispersion with the final concentration of 0.05 mg/mL The tubes were returned to incubator at 52 °C and placed in the minishaker (VMR) at a speed of 100 rpm for 1 h. The obtained wrapping system was directly used for viability test and photosynthesis. For structural characterization, the excess MOF in the media was removed by centrifugation at 140 × *g* for 30 min. The supernatant was collected and the centrifugation was repeated three times. The salts in the obtained supernatant were removed by further centrifugation at 2,500 rpm for 20 min. The precipitate was collected and the centrifugation was repeated three times. Finally, the precipitate was redispersed in water for structural characterization.

Fluorescent Labeling of MOF Monolayer. Molecules containing carboxylate groups can bind to the MOF monolayer through the coordination bond between carboxylate moieties and zirconium clusters. For this purpose, 2-FITC-biphenyl-4,4′-dicarboxylic acid (FITC-H_2BPDC) was synthesized according to reported literature (27). To functionalize the MOF monolayer with FITC-H_2BPDC, 20 mg of FITC-H_2BPDC was added into a solution of MOF (5 mg) in DMF (5 mL). The mixture was incubated at 85 °C for 24 h before washing repeatedly by centrifugation in DMF and water. The final MOF monolayer functionalized with FITC-BPDC was redispersed in water for further usage.

Synthesis of Model Compound ZrDMPO. A mixture of $ZrCl_4$ (10 mg) and dimethylphosphate (30 mg) in DMF (2 mL) was incubated at 85 °C for 2 d and rhombohedral single crystals were obtained. The crystals were washed with DMF and acetone before dried under vacuum.

Structural Characterization. TEM samples were prepared by dropping suspensions onto the 400-mesh copper grids with lacey carbon support. The grids were air dried for 1 d. Bright-field TEM imaging was performed on a JEOL 2100-F 200-kV Field-Emission Analytical TEM equipped with Oxford INCA EDS X-ray detection system (Oxford Instruments) at the Molecular Foundry at Lawrence Berkeley National Laboratory (Berkeley, CA). High-angle annular dark-field scanning TEM images and X-ray elemental mapping were acquired with a 1-nm probe at 200 kV. The specimens were tilted 10° toward the X-ray detector to optimize the X-ray detection geometry. Collection time was individually optimized for the best results. SEM samples were prepared by dropping suspensions onto the silicon wafer and air dried for 1 d. SEM images were recorded on a Zeiss Gemini Ultra-55 analytical SEM with accelerating voltage of 5 kV.

Superresolution 3D-structured illumination microscopy imaging was performed on a Zeiss ELYRA PS.1 system (Carl Zeiss). Images were acquired with a Plan-Apochromat 100×/1.40 oil immersion objective and an Andor iXon 885 EMCCD camera. A 10-mW 486-nm optically pumped semiconductor laser (Coherent Inc.) and a BP 510/620-nm emission filter (Optics Balzers AG) were used. Thirty images with 86-nm *z* section were acquired for generating superresolution images. Raw images were reconstructed and processed to demonstrate structure with greater resolution by the ZEN 2011 software (Carl Zeiss), and the Imaris software was used to analyze the reconstructed images.

ICP-AES (Optima 7000 DV; Perkin-Elmer) was used to determine the amount of Zr in the material. The samples were digested in a solution mixture of nitric acid (0.5 mL) and hydrofluoric acid (0.1 mL). The resulting solution was filtered then diluted with 2% aqueous nitric solution to 10 mL before the measurement. All samples for PXRD were dried under vacuum before measurement. PXRD patterns were recorded using a Rigaku Miniflex 600 (Bragg-Brentano geometry, Cu Kα radiation λ = 1.54056 Å) instrument. The FTIR spectra were collected on a Bruker ALPHA FTIR Spectrometer equipped with ALPHA's Platinum attenuated total reflection (ATR) single-reflection diamond ATR module, which can collect IR spectra on neat samples. XPS was obtained using an ultrahigh vacuum PHI 5400 XPS system with a nonmonochromatic Al X-ray source (Kα = 1486.7 eV) operated at 350-W power. Survey XPS spectra were obtained with analyzer pass energy of 178.5 eV and step size of 1 eV. High-resolution spectra of P 2p region were obtained with analyzer pass energy of 35 eV and 0.05-eV energy steps. The binding energy scale was corrected setting C 1s (sp2) peak in 284 eV (*SI Appendix*, Fig. S7). The peak fitting was performed using Casa XPS software.

For SXRD study, a colorless rhombohedral crystal (0.200 mm) was mounted on a Bruker D8 Venture diffractometer equipped with a fine-focus Mo target X-ray tube operated at 40-W power (40 kV, 1 mA) and a PHOTON 100 CMOS detector. The specimen was cooled to 100 K using an Oxford Cryosystem chilled by liquid nitrogen. Bruker APEX2 software package was used for data collection; SAINT software package was used for data reduction; SADABS program was used for absorption correction; no correction was made for extinction or decay. The structure was solved by direct methods in a rhombohedral space group R-3 with the SHELXTL software package and further refined with least-squares method. All nonhydrogen atoms were refined anisotropically; all hydrogen were generated geometrically. The details of crystallography data are shown in *SI Appendix*, Tables S1 and S2.

Cell Viability Under Oxidative Stress. The volumetric cell numbers were determined by the manual counting with a Petroff-Hauser counting chamber. In parallel, the cfu assays were performed by sampling and inoculating 0.1 mL of *M. thermoacetica* and *M. thermoacetica*–MOF suspension into 5 mL of molten (T > 50 °C) agar broth supplemented with 40 mM glucose and 0.1 wt % cysteine. Assay tubes were pressurized to 150 kPa with 80:20 mixture of N_2:CO_2 and incubated vertically at 52 °C. After 3 d of growth, visible white, circular colonies were counted to determine the cfu (mL^{-1}) as a measure of cell number and viability.

The viability of *M. thermoacetica* and *M. thermoacetica*–MOF under different O_2 and H_2O_2 concentration was tested after the heterotrophic growth entered a stationary phase. The sterile O_2 was injected by syringe into the bacteria culture media until volumetric concentrations of 21% were reached in the headspace. H_2O_2 was introduced into the culture media by injection with syringe until concentrations reached 1, 5, and 50 μM. For the control experiment, a dispersion of zirconia nanoparticles (<100-nm particle size; Aldrich) was added into the culture media at a concentration to make the Zr amount comparable to that of the MOF.

The *E. coli*–MOF was prepared in the same way as *M. thermoacetica*–MOF. Zeiss Z1 AxioObserver inverted fluorescence microscope was used for measuring living cell cultures over extended periods of time. It is equipped with low-light digital-image capture for both color and grayscale. The system is completely automated and can be programmed for long-term experiments on living cells. The 100 μL of *E. coli*–MOF was added into CellASIC ONIX plate B04X, which is controlled by CellASIC Onix Microfluidics system to pump slight bacteria into the main culture chamber at certain time points. General bright-field and excited fluorescence-field movies were collected via Hamamatsu 9100–13 EMCCD camera every 4 min under Zeiss definite focus.

Kinetic Study on H_2O_2 Decomposition Catalyzed by the MOF Monolayer. The kinetics of the H_2O_2 decomposition reaction was measured by charging a 100-mL flask with various amount of MOF monolayer and Milli-Q water to make the final volume of 78.4 mL The flask was closed with a rubber septum, and heated in water bath set at specific temperatures under stirring at 750 rpm. After the MOF dispersion reaches the set temperature, 1.6 mL of H_2O_2 (1 mM) was instantly injected into the solution and timing was started. At different time intervals, 2 mL of the reaction mixture was sampled by syringe and filtered through polytetrafluoroethylene membrane (pore size of 200 nm; Whatman). The H_2O_2 concentration in the obtained solution was determined through the Ghormley triiodide method (24, 25), in which I^- is oxidized quantitatively by

H_2O_2 to I_3^-. Specifically, the sample solution was added with 100 μL of 1 M KI, 100 μL of a mixture solution containing 1 M sodium acetate and 1 M acetic acid, and adjusted to the final volume of 2 mL The solution was left to react for 5 min before measuring the absorbance at 350 nm. A solution containing KI, sodium acetate, and acetic acid of the same concentration was prepared in parallel as blank control for background measurement. The molar extinction coefficient of I_3^- at 350 nm was taken as 25,500 $M^{-1}{\cdot}cm^{-1}$ for the calculation of H_2O_2 concentration.

It was reported in the literature (23) that the catalytic decomposition of H_2O_2 on zirconia follows first-order kinetics with respect to H_2O_2. When an excess of zirconia is present, the reaction kinetics can be approached to a pseudo-first order. As such, the concentration of H_2O_2 as a function of reaction time follows

$$\ln\left(\frac{[H_2O_2]}{[H_2O_2]_0}\right) = -k_1 t,$$

where k_1 is the pseudo–first-order rate constant, t is the reaction time, $[H_2O_2]$ is the concentration of H_2O_2 at a reaction time t, and $[H_2O_2]_0$ is the concentration at $t = 0$. It was found that, after the adsorption of H_2O_2 on the surface of MOF reaches equilibrium, its concentration as a function of time shows good agreement with this first-order kinetic behavior (Fig. 4*A*). Calculating the slopes of such linear dependence affords k_1 at different temperatures (*SI Appendix*, Fig. S9*A*), which follows Arrhenius equation

$$\ln(k_1) = -\frac{E_a}{R}\frac{1}{T} + \ln(A),$$

where E_a is the Arrhenius activation energy, R is the gas constant, A is the frequency factor, and T is the absolute temperature. Extracted from this dependence of rate constant on temperature are E_a as 66.50 ± 0.07 kJ mol^{-1} and A to be 2.8 ± 0.1 × 10^6 s^{-1}. By varying the amount of MOF used as catalyst, the second-order rate constant k_2 was obtained by studying the pseudo–first-order rate constant as a function of the surface-area-to-solution-volume ratio of MOF according to

$$k_1 = k_2\left(\frac{S_A}{V}\right),$$

where S_A is the surface area of MOF and V is the volume of the reaction mixture. Using the specific surface area of MOF, S_{MOF}, this equation can be expressed as

$$k_1 = k_2\left(\frac{S_{MOF}[MOF]}{V}\right),$$

where [MOF] denotes the concentration of MOF. Taking S_{MOF} = 883 m^2 g^{-1} (16), the k_2 obtained from the slope of *SI Appendix*, Fig. S9*B* for the reaction at 335 K is $k_2 = 3.26 \pm 0.04 \times 10^{-9}{\cdot}m{\cdot}s^{-1}$. This value represents the intrinsic catalytic activity of MOF to the decomposition reaction of H_2O_2. To compare the catalytic activity between MOF and zirconia, we take k_2 of zirconia at the same temperature as 9.66×10^{-10} m s^{-1} from the literature (23). We further calculate the zirconium atom density of MOF monolayer as 0.91 nm^{-2} and that of (001) facet of monolithic zirconia as 7.5 nm^{-2} according to their crystal structures. By using these values, the k_2 of MOF monolayer normalized by zirconium atom numbers are obtained as $3.6 \times 10^{-27}{\cdot}m^3{\cdot}s^{-1}$, 28 times higher than that of zirconia ($1.3 \times 10^{-28}{\cdot}m^3{\cdot}s^{-1}$). When normalized by mass, compared with zirconia nanoparticle of 5 m^2 g^{-1} in surface area (23), the k_2 of MOF monolayer is 600 times higher.

Photosynthesis. The *M. thermoacetica*-CdS was prepared as the previous method (6). Typically, 1 mM $Cd(NO_3)_2$ was added to the *M. thermoacetica* when OD_{600} reached 0.42. After 3 d of growth, the opaque yellow suspension revealed the formation of *M. thermoacetica*-CdS. The MOF cytoprotected PBS was prepared in the same way as shown above. Before photosynthesis, 0.2 wt % cysteine was added to each tube. The sterilized O_2 was injected into each tube until 2% (vol/vol) to mimic the oxidative stress condition in the whole reaction. Each tube was stirred at 150 rpm and heated to a measured temperature of 55 °C by a stirring hot plate. The illumination source employed for simulated sunlight measurements was a collimated 75-W Xenon lamp (Newport, Corp.) with an AM 1.5 G filter. All light intensities were calibrated by a silicon photodiode (Hamamatsu S1787-04). Concentrations of photosynthetic products were measured by ^{1}H-qNMR with sodium 3-(trimethylsilyl)-2,2′,3,3′-tetradeuteropropionate (TMSP-d_4; Cambridge Isotope Laboratories, Inc.) as the internal standard in D_2O. Spectra were processed using the MestReNova software.

Statistical Analysis. All data are expressed as mean ± SD. Each experiment was repeated at least three times.

ACKNOWLEDGMENTS. We thank J. Baek and B. Rungtaweevoranit (O.M.Y. group) for the acquisition of XPS data and SEM images, C. Zhao (O.M.Y. group) for help in mechanistic studies of H_2O_2 decomposition by MOF, C. S. Diercks (O.M.Y. group) for discussions, and C. Chen (P.Y. group) for cell culture and enumeration. SEM, XPS, and STEM measurements were performed at the Molecular Foundry, Lawrence Berkeley National Laboratory. This research was supported by BASF SE (Ludwigshafen, Germany) for synthesis and characterization of MOFs, by King Abdulaziz City for Science and Technology (Center of Excellence for Nanomaterials and Clean Energy Applications) for mechanistic studies, and by NASA, Center for the Utilization of Biological Engineering in Space, under Award NNX17AJ31G for bacteria study. H.Z. acknowledges the Suzhou Industry Park Fellowship.

1. Zeikus JG (1980) Chemical and fuel production by anaerobic bacteria. *Annu Rev Microbiol* 34:423–464.
2. Torella JP, et al. (2015) Efficient solar-to-fuels production from a hybrid microbial-water-splitting catalyst system. *Proc Natl Acad Sci USA* 112:2337–2342.
3. Liu C, et al. (2015) Nanowire-bacteria hybrids for unassisted solar carbon dioxide fixation to value-added chemicals. *Nano Lett* 15:3634–3639.
4. Nichols EM, et al. (2015) Hybrid bioinorganic approach to solar-to-chemical conversion. *Proc Natl Acad Sci USA* 112:11461–11466.
5. Liu C, Colón BC, Ziesack M, Silver PA, Nocera DG (2016) Water splitting-biosynthetic system with CO_2 reduction efficiencies exceeding photosynthesis. *Science* 352:1210–1213.
6. Sakimoto KK, Wong AB, Yang P (2016) Self-photosensitization of nonphotosynthetic bacteria for solar-to-chemical production. *Science* 351:74–77.
7. Sakimoto KK, Zhang SJ, Yang P (2016) Cysteine–cystine photoregeneration for oxygenic photosynthesis of acetic acid from CO_2 by a tandem inorganic–biological hybrid system. *Nano Lett* 16:5883–5887.
8. Karnholz A, Küsel K, Gössner A, Schramm A, Drake HL (2002) Tolerance and metabolic response of acetogenic bacteria toward oxygen. *Appl Environ Microbiol* 68:1005–1009.
9. Ai H, Fang M, Jones SA, Lvov YM (2002) Electrostatic layer-by-layer nanoassembly on biological microtemplates: Platelets. *Biomacromolecules* 3:560–564.
10. Liang K, et al. (2016) Metal–organic framework coatings as cytoprotective exoskeletons for living cells. *Adv Mater* 28:7910–7914.
11. Liang K, et al. (2017) An enzyme-coated metal–organic framework shell for synthetically adaptive cell survival. *Angew Chem Int Ed Engl* 56:8510–8515.
12. Liu Z, Xu X, Tang R (2016) Improvement of biological organisms using functional material shells. *Adv Funct Mater* 26:1862–1880.
13. Park JH, et al. (2014) Nanocoating of single cells: From maintenance of cell viability to manipulation of cellular activities. *Adv Mater* 26:2001–2010.
14. Yang SH, et al. (2009) Biomimetic encapsulation of individual cells with silica. *Angew Chem Int Ed Engl* 48:9160–9163.
15. Elani Y, et al. (2018) Constructing vesicle-based artificial cells with embedded living cells as organelle-like modules. *Sci Rep* 8:4564.
16. Cao L, et al. (2016) Self-supporting metal–organic layers as single-site solid catalysts. *Angew Chem Int Ed Engl* 55:4962–4966.
17. Wang Z, et al. (2017) Organelle-specific triggered release of immunostimulatory oligonucleotides from intrinsically coordinated DNA-metal-organic frameworks with soluble exoskeleton. *J Am Chem Soc* 139:15784–15791.
18. Heptinstall S, Archibald AR, Baddiley J (1970) Teichoic acids and membrane function in bacteria. *Nature* 225:519–521.
19. Brown S, Santa Maria JP, Jr, Walker S (2013) Wall teichoic acids of gram-positive bacteria. *Annu Rev Microbiol* 67:313–336.
20. Kim H, Keller SW, Mallouk TE (1997) Characterization of zirconium phosphate/polycation thin films grown by sequential adsorption reactions. *Chem Mater* 9:1414–1421.
21. Boga HI, Brune A (2003) Hydrogen-dependent oxygen reduction by homoacetogenic bacteria isolated from termite guts. *Appl Environ Microbiol* 69:779–786.
22. Das A, Silaghi-Dumitrescu R, Ljungdahl LG, Kurtz DM, Jr (2005) Cytochrome *bd* oxidase, oxidative stress, and dioxygen tolerance of the strictly anaerobic bacterium *Moorella thermoacetica*. *J Bacteriol* 187:2020–2029.
23. Lousada CM, Johansson AJ, Brinck T, Jonsson M (2012) Mechanism of H_2O_2 decomposition on transition metal oxide surfaces. *J Phys Chem C* 116:9533–9543.
24. Ghormley JA, Stewart AC (1956) Effects of γ-radiation on ice. *J Am Chem Soc* 78:2934–2939.
25. Diesen V, Jonsson M (2014) Formation of H_2O_2 in TiO_2 photocatalysis of oxygenated and deoxygenated aqueous systems: A probe for photocatalytically produced hydroxyl radicals. *J Phys Chem C* 118:10083–10087.
26. Lousada CM, Jonsson M (2010) Kinetics, mechanism, and activation energy of H_2O_2 decomposition on the surface of ZrO_2. *J Phys Chem C* 114:11202–11208.
27. Schrimpf W, et al. (2018) Chemical diversity in a metal-organic framework revealed by fluorescence lifetime imaging. *Nat Commun* 9:1647.